Available online at www.sciencedirect.com
SCIENCE DIRECT®
Pergamon
Acta Materialia 51 (2003) 87–99
Acta MATERIALIA
www.actamat-journals.com

A nanoindentation study of serrated flow in bulk metallic glasses

C.A. Schuh *, T.G. Nieh

Materials Science and Technology Division, Lawrence Livermore National Laboratory, Livermore, CA, 94550, USA

Received 1 May 2002; received in revised form 29 July 2002; accepted 30 July 2002

Abstract

Plastic deformation of two Pd- and two Zr-based bulk metallic glasses (BMGs) is investigated through the use of nanoindentation, which probes mechanical properties at the length scale of shear bands, the carriers of plasticity in such alloys. These materials exhibit serrated flow during nanoindentation, manifested as a stepped load-displacement curve punctuated by discrete bursts of plasticity. These discrete "pop-in" events correspond to the activation of individual shear bands, and the character of serrations is strongly dependent on the indentation loading rate; slower indentation rates promote more conspicuous serrations, and rapid indentations suppress serrated flow. Analysis of the experimental data reveals a critical applied strain rate, above which serrated flow is completely suppressed. Furthermore, careful separation of the plastic and elastic contributions to deformation reveals that, at sufficiently low indentation rates, plastic deformation occurs entirely in discrete events of isolated shear banding, while at the highest rates, deformation is continuous, without any evidence of discrete events at any size scale. All of the present results are consistent with a kinetic limitation for shear bands, where at high rates, a single shear band cannot accommodate the imposed strain rapidly enough, and consequently multiple shear bands must operate simultaneously.

1. Introduction

Bulk metallic glasses (BMGs) are collectively considered as emerging structural materials due to their high strength and large elastic deflection prior to the onset of plastic deformation. However, plastic deformation of these alloys is highly localized into shear bands, which can propagate across macroscopic specimen dimensions on millisecond time scales [1–12]. Because of the dominance of shear banding in low-temperature plasticity, these alloys exhibit several unique deformation phenomena. First, plasticity in BMGs deviates from the classical von Mises yield criterion, perhaps exhibiting a Mohr-Coulomb yield criterion that is sensitive to both the shear and normal stress components in the plane of shear [1,4,13–18]. Consequently, for uniaxial deformation the plane of shear yielding is not inclined at 45° to the tensile axis, but at a slightly different angle that is specific to the alloy composition [1,14,17]. Second, tensile deformation

* Corresponding author. Tel.: +1-617-452-2659; fax: +1-617-252-1175. Massachusetts Institute of Technology, Materials Science and Engineering, Room 8-211, Cambridge, MA 02139, USA.
E-mail address: schuh@mit.edu (C.A. Schuh).

1359-6454/03/$22.00
doi:10.1016/S1359-6454(02)00303-8

leads to abrupt brittle fracture due to shear-off along a single plane [14,17,19,20].

Third, although plastic deformation is possible in constrained modes of loading (e.g., compression), BMGs exhibit essentially no strain hardening, and plastic flow is serrated, with many small load drops that correspond to the activation of individual shear bands. [1,3,4,9,10,21].

Because the peculiar mechanical traits described above may limit the forming or application of BMGs, there have been many investigations of deformation, fracture, and shear banding in various BMG alloys. At room temperature, several investigators have addressed the nature of the yield criterion, by measuring the shear angle in tension or compression [1,14,17], or by examining yield under varying stress states [4,14,16]. Recently, Vaidyanathan et al. [18] have combined finite element modeling with instrumented indentation to assess the yield criterion of a Zr-based BMG. The phenomenon of serrated flow has been investigated in considerable detail for a Pd-16Si-6Cu alloy by Kimura and Masumoto, who performed experiments in compression [10], mode I crack opening [7,8], and mode III crack tearing [5,6]. These authors found that serrated flow exhibited similar features in all three of these loading configurations, and correlated each displacement serration with an observation of shear band activity on the specimen surface. By varying the rate of loading, these authors further observed that high deformation rates tend to suppress serrated flow, and above some critical displacement rate serrated flow could not be observed. Using mechanical models of their testing geometries [10], Kimura and Masumoto also corrected the serration amplitudes to account for elastic response of the test apparatus.

Serrated flow and the Mohr-Coulomb yield criterion are direct consequences of shear banding; a better understanding of these phenomena can be gained by study of the physical nature of shear bands. For example, Neuhäuser [22] has used high-speed cinematography to approximate the propagation rates of shear bands in an iron-based BMG. Spatially-resolved thermal measurements such as those employed by Flores and Dauskardt [23] can shed light on the important issue of adiabatic heating during deformation of BMGs, which may cause melting or crystallization in or near shear bands [17]. Pekarskaya et al. [12] have used transmission electron microscopy (TEM) to investigate the atomic-scale nature of shear bands in a deforming BMG-matrix composite, and noted that shear bands are not restricted to a single plane. Finally, Kim et al. [24] have recently reported TEM observations on an indented Zr-based BMG, and found that deformation induced crystallization of the alloy on a fine scale around the indent. These studies all suggest that shear banding in BMGs may involve complex thermal and structural changes.

In recent work by Wright et al. [1] and Golovin et al. [25], nanoindentation has been proposed as a method for the study of serrated flow in BMGs. The former authors observed that the onset of plasticity during nanoindentation of a Zr-based BMG occurred at a discrete displacement burst (a “pop-in”). This result has an analog in indentation of crystalline materials, which exhibit such bursts when dislocations are nucleated. [26–30] However, apart from the initial discontinuity in the load-displacement curve, Wright et al. [1] did not observe further flow serrations at higher loads. In nanoindentation studies of Pd-30Cu-10Ni-20P, Golovin et al. [25] observed numerous displacement bursts through the full loading history of the indent. They further correlated the number of pop-in events directly with the number of shear bands observed on the specimen surface around the indent. The works of Suresh and co-workers [18,24] also demonstrate that shear bands form around indents, and show how coupled mechanical and microscopic investigations of nanoindented BMGs may be a powerful probe into the nature of shear banding.

In a recent preliminary report, we described observations of serrated flow in a Pd-40Ni-20P BMG during instrumented nanoindentation [31]. We showed that serrated flow is strongly dependent on the indentation strain rate, with lower rates promoting more prominent serrations or displacement bursts. In the present work, we expand on that initial report by considering serrated flow of four different BMG materials, two Pd-based and two Zr-based alloys. We find that rate-dependent serrated flow (as we initially reported in Pd-40Ni-20P) is common to all of these materials, although the transition from serrated to non-serrated flow

varies with composition. We also show that the observed rate effects represent a transition from continuous yielding (at high rates) to completely discrete yielding (at low rates), where all of the plasticity can be ascribed to individual load serrations.

2. Experimental

Four BMG compositions were studied, including Pd-40Ni-20P, Pd-30Cu-10Ni-20P, Zr-10Al-14.6Ni-17.9Cu-5Ti, and Zr-10Al-10Ni-15Cu, where compositions are listed in atomic %. Three of the alloys were all prepared by casting methods, as described in more detail elsewhere (Pd-40Ni-20P [20,31,32], Pd-30Cu-10Ni-20P [32], and Zr-10Al-14.6Ni-17.9Cu-5Ti [33–35]). The Zr-10Al-10Ni-15Cu alloy was prepared by consolidation of glassy powders in the supercooled liquid region, through a process of warm-extrusion [36]. In all cases, the amorphous nature of the alloy was confirmed by x-ray diffraction, as also described in the references listed above. Prior to indentation experiments, each BMG was mechanically polished to a mirror finish.

Nanoindentation experiments were conducted using a TriboIndenter instrumented nanoindenter (from Hysitron, Minneapolis, MN), calibrated on pure aluminum and silica. The indenter tip was conical with a blunt tip radius of 450 nm, giving essentially spherical contact surfaces for most of the indents performed here. Indentations were performed in load-control mode to loads as high as 10 mN using loading rates from 0.02 to 300 mN/s, and data acquisition rates as high as 6000 points per second were used to capture the dynamics of serrated yielding. The loading rates used in this work are bounded by experimental limitations; very slow loading rates are complicated by thermal and electronic drift, while data acquisition rates are insufficient to resolve extremely rapid events.

3. Results

Load-displacement (*P-h*) curves for nanoindentations on each of the four experimental materials are presented in Fig. 1. In this figure the origin of each curve has been displaced so that multiple curves can be accommodated on each graph, and only the loading portions of the *P-h* curves are shown for clarity. The results in Fig. 1a are for the Pd-40Ni-20P alloy, and typify the general trends observed for all of the materials in this study. At low loading rates, the *P-h* curves are punctuated by many discrete bursts of rapid displacement at nearly constant load. This behavior is analogous to serrated flow observed in compression tests on the same alloy [4], where plastic deformation is punctuated by many load drops at constant strain. In displacement controlled compression experiments, each serration corresponds to the operation of a single shear band that quickly accommodates the applied strain, giving rise to a load drop. In our indentation experiments, the indentation load is controlled, so the activation of a shear band gives rise to a burst of displacement. We note that a similar result to that shown in Fig. 1 has been reported for serrated flow in solid-solution aluminum alloys during indentation [37–39], although those alloys were fully crystalline, and serrated flow results from solute-dislocation interactions. However, several different research groups using different nanoindenters have also noted load serrations during indentation of BMGs [25,40,41].

In Fig. 1, we find that the displacement in each strain burst is a function of the instantaneous depth of the indenter; larger indents produce larger pop-in events. This effect is illustrated for the Pd-40Ni-20P BMG in Fig. 2, which further demonstrates that the scaling is approximately linear. This result is a natural consequence of the increasing length scale of the indentation geometry as the depth increases. Since a single shear band can produce displacements as large as several microns, we expect that larger pop-ins correspond to greater shear displacements within the shear band.

Although serrated flow is observed clearly at low indentation loading rates, the additional *P-h* curves in Fig. 1 demonstrate a rate dependence of the serration character. This trend is typified by the results in Fig. 1a for the Pd-40Ni-20P alloy. As the loading rate is increased across several orders of magnitude, the nature of serrated flow changes dramatically, from ideal stair-step-like *P-h* curves at

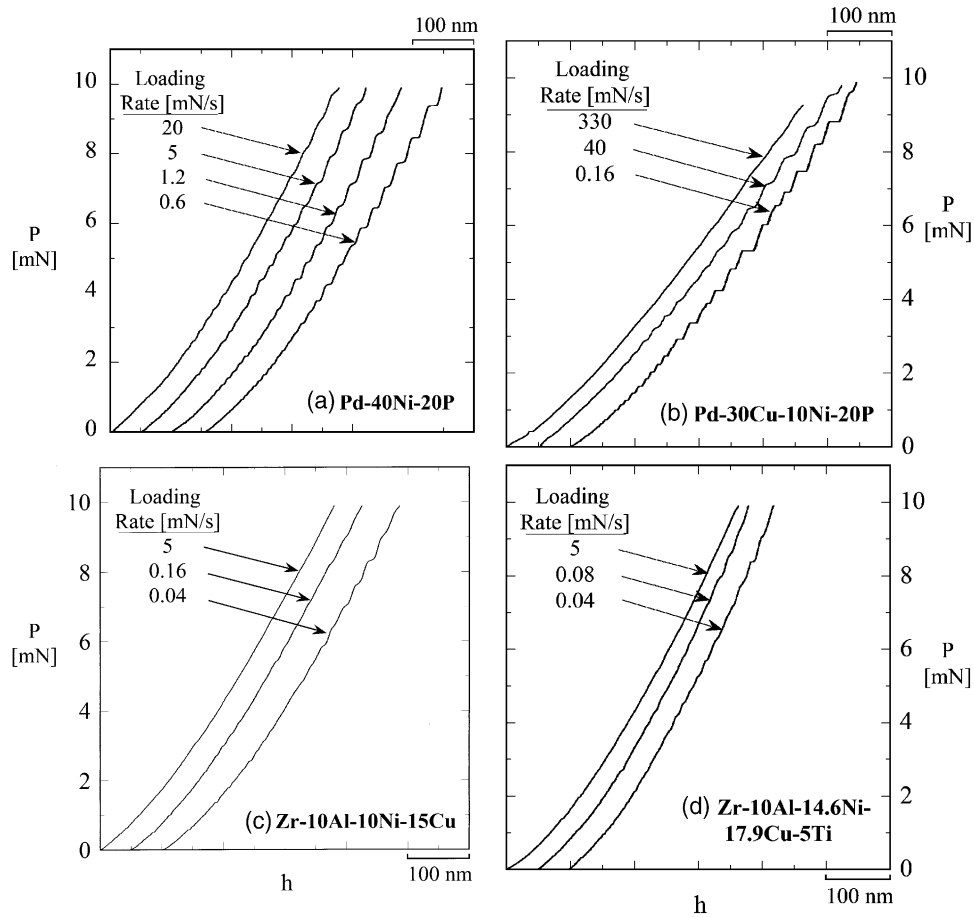

Fig. 1. Typical load-displacement (*P-h*) curves measured on the loading portion of nanoindentation experiments, for all four of the BMG compositions investigated. Curves are offset from the origin for clear viewing, and the rate of indentation loading is specified in each graph.

the lowest rates, to very smooth parabolic curves at the highest rates. At rates in between these extremes, the *P-h* curves exhibit serrations that appear more as fluctuations or ripples than as discrete, horizontal displacement bursts. Additionally, this trend is not limited to the Pd-40Ni-20P alloy, but is found to be a general feature of indentation loading in the four BMGs studied here, as indicated in Fig. 1b–c. The character of serrated flow appears different among the various compositions; the Pd-based glasses seem to exhibit more sharp displacement bursts, while the Zr-based materials have generally smoother curves at similar rates. Finally, although the nature of serrated flow in Fig. 1 is loading rate dependent, the general shape of the *P-h* curves are quite similar at all loading rates, suggesting a rate independent hardness or strength. This result is in agreement with the uniaxial yield stress data compiled by Mukai et al. [20] for several different Pd- and Zr-based BMGs.

4. Discussion

The results in Fig. 1 illustrate a strong rate dependence of serrated flow in four BMGs, which may have important implications for structural application of these materials. In the following sections we first quantify this rate dependence in terms of the equivalent strain rate during nanoindenta-

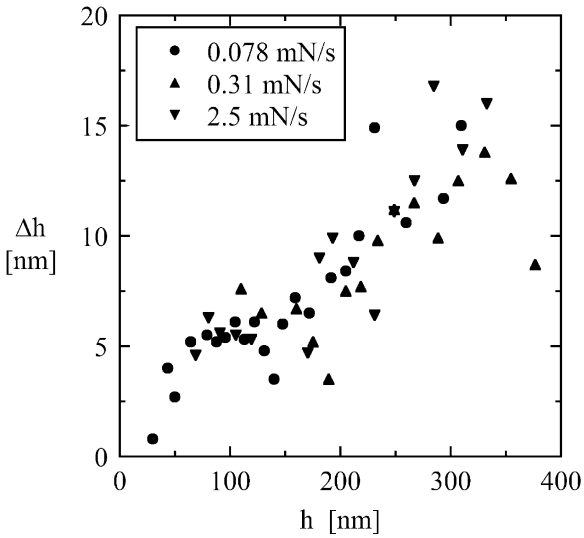

Fig. 2. The scaling of pop-in depth (Δh) with the instantaneous indentation depth (h) for Pd-30Cu-10Ni-20P.

tion, and assess the contribution of serrated flow to the total plastic response of the BMGs. Finally, we discuss the possible physical origin of the results, as well as implications of these experiments.

4.1. Strain rate sensitivity of serrated flow

During nanoindentation with a constant loading rate, the displacement rate is a non-linear function of time, as is the indentation strain rate, which is defined as [42–44]:

$$\dot{\varepsilon}_i = \frac{1}{h}\cdot\frac{dh}{dt} \tag{1}$$

where t is time. In Fig. 3, the indentation strain rate is plotted as a function of depth for (a) Pd-30Cu-10Ni-20P, and (b) Zr-10Al-10Ni-15Cu. Although not shown here, a similar graph is available for Pd-40Ni-20P in Ref. [31], and the curves for the Zr-10Al-14.6Ni-17.9Cu-5Ti alloy are similar to those shown in Fig. 3b for Zr-10Al-10Ni-15Cu. At the outset of each experiment, the strain rate is effectively infinite, since Eq. (1) is singular at $h = 0$. However, at finite depths the strain rate decreases as $\sim 1/h$, approaching an approximately constant value for very large depths. As Fig. 3 illustrates, the trends in strain rate are not monotonic, as would be expected simply on the basis of Eq. (1), but exhibit many short peaks in strain rate that appear to increase in size as the indentation proceeds. These short bursts of rapid displacement are the same pop-in events exhibited in the *P-h* curves of Fig. 1, and the peaks in Fig. 3 are found to correlate exactly with the load serrations in Fig. 1. These peaks are more pronounced in the Pd-based (Fig. 3a) than the Zr-based BMGs (Fig. 3b), and their magnitude is strongly affected by the indentation strain rate, as also observed in Fig. 1.

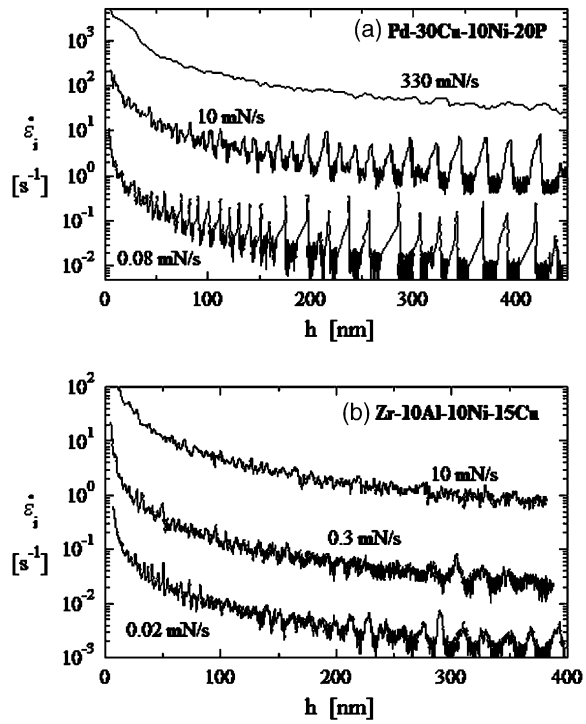

Fig. 3. The indentation strain rate plotted as a function of the indentation depth for (a) Pd-30Cu-10Ni-20P and (b) Zr-10Al-10Ni-15Cu alloys, with the loading rate indicated by each curve. Strain rate peaks are observed at the lower loading rates, and correspond to the pop-in events observed in Fig. 1.

The prominence of serrated flow can be quantified using the non-dimensional height, *A*, of the peaks in Fig. 3, defined as:

$$A = \frac{\dot{\varepsilon}_i^{max}}{\dot{\varepsilon}_i^{base}}, \tag{2}$$

where the superscripts refer to either the maximum strain rate at the height of the peak (max), or the

baseline or 'background' strain rate surrounding the peak (base). The value of A thus represents the factor by which deformation is accelerated during an isolated pop-in or serration. As Fig. 3 illustrates, peaks can only be clearly differentiated from the background at indentation depths greater than about 50–100 nm, due to the ~1/h dependence of the applied strain rate. Accordingly, values of A cited below are all acquired at $h > 100$ nm depths.

Fig. 4 illustrates the change in serrated flow prominence (A) with indentation strain rate, where each data point corresponds to a single serration peak (as shown in Fig. 3). Each of the four BMG materials is represented on a separate graph for clearer representation, though all four data sets exhibit the same general trends. At low applied strain rates, serrations are very prominent, and instantaneously accelerate the deformation by as much as one or two orders of magnitude (for the Zr- and Pd-based BMGs, respectively). As the

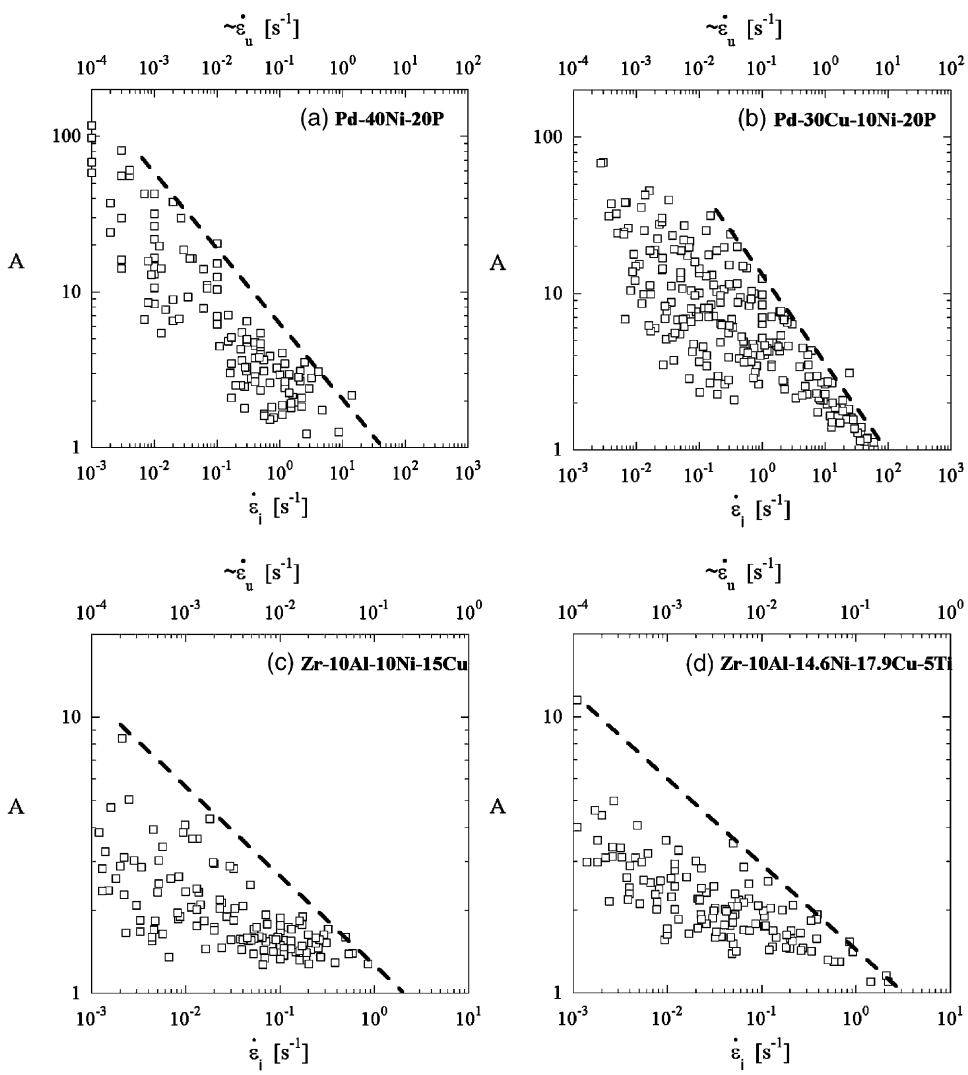

Fig. 4. The height, A, of strain rate "peaks" during pop-in events (as in Fig. 3), which represents the factor by which deformation is accelerated during such events. Here A is plotted as a function of the instantaneous indentation strain rate; the upper x-axis also shows the approximate uniaxial equivalent strain rate.

applied strain rate is increased, the height of the serration peaks decreases in a systematic fashion, such that most of the data points lie beneath the dashed lines in Fig. 4. Below these lines, the data are broadly scattered, indicating that the rate of serrated flow is not solely determined by the strain rate, but may depend on some stochastic parameter such as the local atomic arrangements (i.e., short- or medium-range geometric or chemical ordering [45,46]) within the BMG. However, an increase in indentation rate invariably reduces the maximum measured peak heights, and above some threshold strain rate, serration peaks are no longer observed. For the four BMGs studied here, the transition from serrated to smooth flow occurs at different strain rates, as discussed in more detail below.

The indentation strain rate described by Eq. (1) simplifies a multiaxial deformation problem with a single, characteristic strain rate. For comparison with other studies performed in uniaxial loading, it is necessary to relate $\dot{\varepsilon}_i$ to the equivalent uniaxial strain rate, $\dot{\varepsilon}_u$. Although this relationship has been considered by many previous authors within the context of indentation creep [42–44,47–49], no simple relationship is available that is valid for all materials and indenter tips. Here we use the relationship determined experimentally by Poisl et al. [44], who performed indentation creep experiments on another amorphous metal, Se, and compared the indentation results directly to tensile creep data for the same material. They proposed that:

$$\dot{\varepsilon}_u = C \cdot \dot{\varepsilon}_i, \tag{3}$$

where the constant $C = 0.09$. Thus, indentation strain rates are about one order of magnitude higher than the equivalent uniaxial strain rate. In Fig. 4, the upper axis is scaled by the factor C, to show the approximate uniaxial strain rates for the present experiments.

The results in Fig. 4 illustrate that serrated flow in BMGs is suppressed above some critical strain rate, in the range of $\dot{\varepsilon}_u \approx 10^{-1}$ to 10^{1} s^{-1}. This result is summarized in Fig. 5, which maps the occurrence of serrated and non-serrated indentation experiments for all four of the experimental materials, and also compares the present results with several literature studies of various BMGs. In this figure, the solid symbols indicate an observation of serrated flow, while open symbols represent observations of smooth yielding without load serrations. As the figure shows, our observation of a maximum strain rate for serrated flow is broadly consistent with isolated data points from the literature, from experiments conducted in compression and indentation. We note that the available indentation investigations [25,41] of serrated flow did not explicitly study the strain rate as discussed above, so the average strain rate is estimated from the total depth and duration of their indents.

The most detailed prior study of serrated flow as a function of strain rate is that of Kimura and Masumoto [5–8,10] on a different BMG not studied here, Pd-16Si-6Cu. In compression [10] crack-opening [7,8] and crack-tearing [5,6] modes of loading, these authors demonstrated that serrated flow was most common at low applied displacement rates, and was suppressed at higher rates. For their experiments in compression, a critical threshold strain rate of about $\sim 3 \cdot 10^{-2}$ s^{-1} can be identified, as illustrated in Fig. 5. The present data for the Pd-based BMGs exhibit the same effect during nanoindentation loading, although the critical strain rate is found to be dependent on composition. Our results for Pd-40Ni-20P are also in agreement with experiments by Mukai et al. [20,50] and Donovan [4] on the same alloy, and span a range of strain rates not previously accessed by those studies. Likewise, the recent indentation study of Golovin et al. [25] on Pd-30Cu-10Ni-20P suggests a similar trend to that found here. Those authors found fewer load serrations for indentations performed more quickly, although they did not determine the strain rate of their experiments explicitly and the values in Fig. 5 are only approximate.

Data on serrated flow of Zr-based alloys are less common, although the experiments of Wright et al. [1,9] as well as Lam and Chong [41] describe serrated flow of a Be-containing BMG at low strain rates (at or below 10^{-2} s^{-1}). Nonetheless, our results agree with these studies, and further show that serrated flow in Be-free Zr-based BMGs occurs at rates up to about 10^{-1} s^{-1}. In the following section, we further explore this rate-depen-

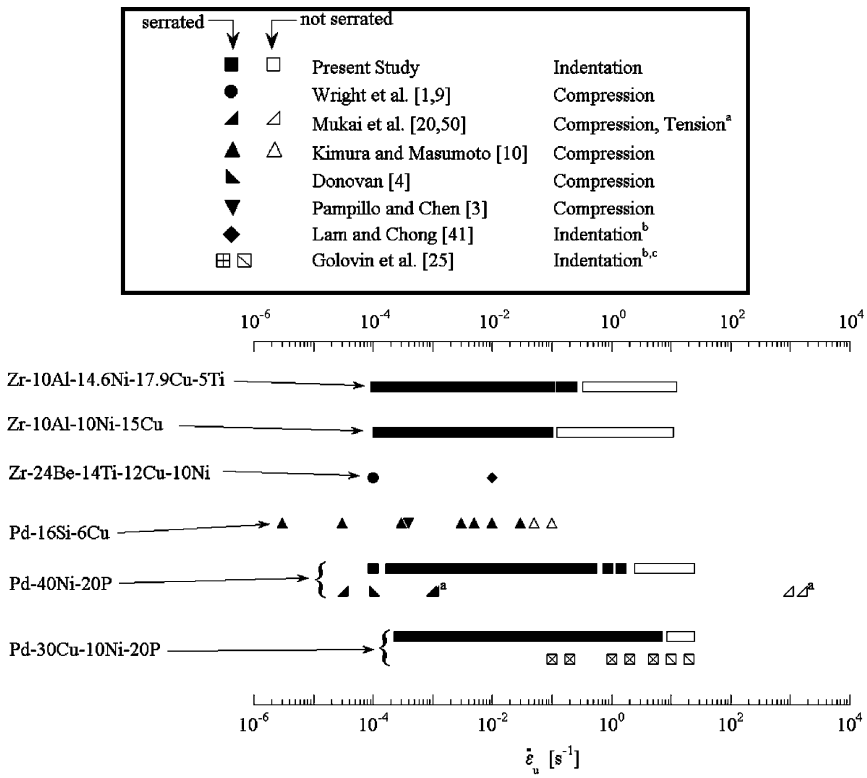

Fig. 5. Compilation of the present indentation results, showing the range of strain rates over which serrated flow is and is not observed. Data from the literature are also assembled, illustrating the same general trends found in this work, in several different modes of loading. Notes: (a) tensile data that show single shear bands (solid triangles) or multiple shear bands (open triangles), (b) strain rates are approximated from literature indentation studies with Eqs. (1) and (3), using the total depth and test duration to calculate the indentation rate, (c) crossed squares represent tests with many (i.e., > 2) serrations, while slashed squares correspond to indentations with 2 or less serrations.

dence, and assess the contribution of load serrations to the total plastic response of the BMGs; the physical origin of our results is discussed in a later section.

4.2. Transition from discrete to continuous yielding

The strain rate dependency of serrated flow described above represents a transition from discrete to continuous plastic deformation, although whether or not plasticity can be completely ascribed to the observed serrations remains uncertain. In this section, we analyze the data to reveal the contribution of load serrations (individual shear band activity) to the plastic deformation of the four experimental BMG materials.

Fig. 6 shows a single *P-h* curve obtained at a loading rate of 0.08 $mN \cdot s^{-1}$ on the Pd-30Cu-10Ni-20P alloy, including the elastic unloading portion of the curve. After removal of the indenter tip, the recovered elastic depth is found as $h_e \approx 208$ nm. The contribution of discrete shear bands to plastic deformation of the alloy can be assessed following the method of Gouldstone et al. [29] who describe the construction of a "consolidated elastic" loading curve, obtained by removing all of the pop-in discontinuities from the loading portion of the *P-h* curve. This procedure essentially corrects the experimental *P-h* curve by discounting the plastic deformation associated with serrated flow, producing a smooth and continuous curve, as illustrated by the arrows in Fig. 6. At its maximum, this consolidated curve exhibits a depth of $h'_e \approx 223$ nm,

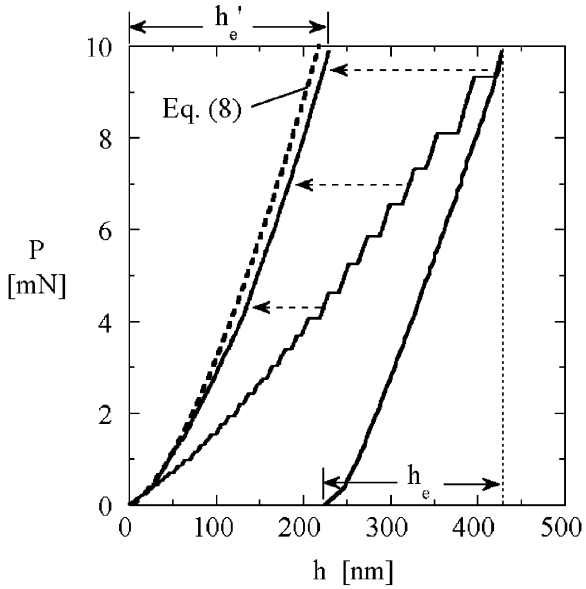

Fig. 6. An example of a serrated *P-h* curve for the Pd-30Cu-10Ni-20P alloy, showing both the elastic-plastic loading and elastic unloading curve. After removal of the pop-in discontinuities, a smooth "consolidated elastic" curve is obtained (as denoted by the arrows), which is in good agreement with the predictions for a purely elastic contact (Eq. (8), dashed line).

which is close to the true elastic depth measured on unloading, $h_e \approx 208$ nm. This result indicates that essentially all of the plastic strain experienced by the BMG during nanoindentation occurs in discrete bursts, due to the motion of individual shear bands.

The above result can be further validated by considering the theoretical elastic curve that would be expected in the absence of plastic flow. The theoretical elastic curve is described by the following load-displacement relationship [51]:

$$\frac{dP}{dh} = \frac{2}{\sqrt{\pi}} \cdot E_r \cdot \sqrt{A_p} \tag{4}$$

where A_p is the projected contact area and the reduced biaxial modulus, E_r, is given by:

$$\frac{1}{E_r} = \frac{(1-\nu_i^2)}{E_i} + \frac{(1-\nu_s^2)}{E_s} \tag{5}$$

where E is the Young's modulus, ν is the Poisson's ratio, and the subscripts refer to the indenter (i) or the substrate (s). Assuming a spherical indenter within the limit of small elastic strains, Eq. (4) reduces exactly to the Hertzian contact theory [52]. For the present geometry, the projected contact area is given by:

$$A_p = \pi \cdot (2 \cdot R \cdot h_c - h_c^2) \tag{6}$$

where $R = 450$ nm is the radius of the indenter tip, and h_c is the vertical depth of the indent along which contact is made. This latter quantity is not equal to the measurement depth, h, because the specimen surface deflects elastically around the indenter. As described in detail in Ref. [51], the elastic analysis of Sneddon (see, e.g., Ref. [52]) can be used to determine the true contact depth as:

$$h_c = h \cdot \Delta_p = h \cdot \left(1 - \frac{\varepsilon}{2}\right) \tag{7}$$

where the parameter Δ_p is given in terms of the dimensionless quantity ϵ defined in Ref. [51], which is approximately $\varepsilon \approx 0.75$.

By introducing Eqs. (6) and (7) into Eq. (4), separating the variables, integrating, and recognizing that Δ_p, R, and h are all positive, the following closed-form expression for the *P-h* relationship is derived:

$$P = \frac{E_r}{\Delta_p} \cdot \left[(\Delta_p \cdot h - R) \cdot \sqrt{2 \cdot R \cdot \Delta_p \cdot h} + \frac{\pi}{2} \cdot R^2 - R^2 \cdot \arctan\left(\frac{R - \Delta_p \cdot h}{\sqrt{2 \cdot R \cdot \Delta_p \cdot h}} \right) \right] \tag{8}$$

In Fig. 6, the predictions of Eq. (8) for the Pd-30Cu-10Ni-20P alloy are plotted for comparison with the experimental consolidated elastic *P-h* curve. Here we have used a value of $E_r = 104$ GPa, based on Eq. (5) and the elastic constants from Refs. [25,53]; we found the same value experimentally by analyzing the unloading curves by the method of Oliver and Pharr [51]. As seen in Fig. 6, the prediction of Eq. (8), based on purely elastic loading, is in very good agreement with the consolidated elastic curve determined experimentally. This conformity between experiment and elastic contact theory further demonstrates that the plastic deformation sustained during nanoindentation can be wholly attributed to pop-in events. Although prior research has shown that single

shear band propagation produces load serrations in BMGs, the present results confirm that, at sufficiently slow rates of loading, discretized shear band activity is the only source of plastic strain in the Pd-30Cu-10Ni-20P alloy.

Although the results from Fig. 6 illustrate that plasticity is a completely discrete phenomenon at low loading rates, the *P-h* curves in Fig. 1 at higher rates show an absence of this discrete, serrated yielding. In fact, the *P-h* curves at the highest rates for the same alloy (Pd-30Cu-10Ni-20P, Fig. 1b) are conspicuously devoid of obvious pop-in discontinuities, so that a consolidated elastic curve cannot be extracted from the data. This is illustrated in more detail in Fig. 7, where the consolidated elastic *P-h* curves obtained at different indentation rates are shown for the Pd-30Cu-10Ni-20P alloy, and again compared with the theoretical elastic curve predicted by Eq. (8). The lowest loading rate data (0.08 $mN \cdot s^{-1}$) are the same as shown in Fig. 6, which match well with the predicted elastic curve. However, as the loading rate is increased and the experimental *P-h* curves become less serrated (Fig. 1), the consolidated elastic curves deviate increasingly from the ideal curve of Eq. (8). This result demonstrates a dramatic transition, from completely discrete yielding at low rates, to completely continuous yielding at high rates.

The transition from quantized- or discrete-yielding to continuum plastic flow is summarized in Fig. 8, where the fraction of discrete plastic flow is presented as a function of the indentation loading rate. Here the amount of plastic displacement due to discrete pop-in events ($h_{discrete}$) is obtained from the consolidated elastic curves such as shown in Figs. 6 and 7, divided by the true amount of plastic displacement ($h_{plastic}$) that is revealed by the residual depth after unloading of the indent. This ratio represents the fraction of plasticity that can be attributed to discrete shear banding events. Focusing first on the curve for Pd-30Cu-10Ni-20P, we observe that both fully discrete ($h_{discrete}/h_{plastic} \approx 1$) and fully continuum ($h_{discrete}/h_{plastic} \approx 0$) yielding is possible in this alloy during nanoindentation. Furthermore, this transition occurs smoothly over a broad, four-decade range in loading rate.

The trends observed for the Pd-30Cu-10Ni-20P

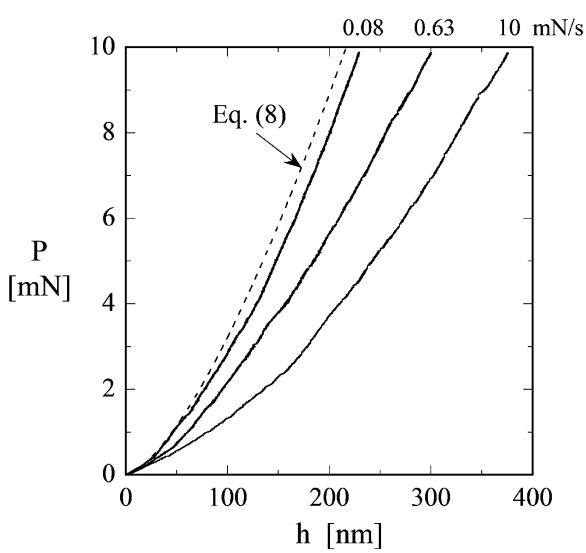

Fig. 7. Consolidated elastic curves for Pd-30Cu-10Ni-20P, determined by removing all of the pop-in discontinuities from the *P-h* curves. As the loading rate is decreased, plastic deformation becomes more discretized into strain burst events, so the consolidated elastic curves approach the limit of ideal elastic contact as given by Eq. (8).

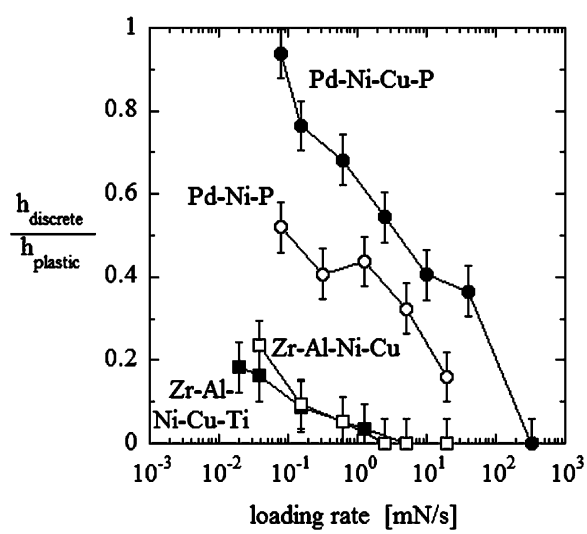

Fig. 8. The ratio of discrete plastic depth ($h_{discrete}$, due to yield serrations) to total plastic depth ($h_{plastic}$), as a function of the indentation loading rate for all four BMG materials. At lower loading rates, this ratio increases toward unity (corresponding to fully discrete plasticity), while higher rates of loading lead to values near zero (corresponding to smooth, continuous yielding).

alloy in Figs. 6–8 are typical of our observations on the three other BMGs in this work. All of the materials exhibit a transition from continuous- toward discrete-yielding as the indentation rate is decreased. However, both of the Zr-based BMGs, as well as the Pd-40Ni-20P alloy, appear to exhibit a broader range over which the transition occurs. For example, below loading rates of ~10 $mN \cdot s^{-1}$, both Zr-based BMGs begin to exhibit discrete plasticity character, but the total strain due to pop-in events does not exceed about 25% of the total plastic strain, even though the loading rate was decreased through an additional 2.5 orders of magnitude (Fig. 8). However, the trend of the data in Fig. 8 is clear, and we expect that at sufficiently slow indentation rates, these BMGs could also exhibit ideal serrated flow, where all of the plastic deformation can be attributed to pop-in events.

4.3. Origin and implications of rate-dependent serrated flow

The disappearance of serrated flow at high strain rates in these BMG materials represents a change in the nature of plastic deformation. We believe that these results (exemplified in Figs. 1, 5 and 8) represent a transition from deformation being carried by a single shear band at low rates, to the simultaneous operation of multiple shear bands at higher rates. Such an observation has been previously reported for Pd-40Ni-20P by Mukai et al. [20], who observed tensile failure along only a single shear band at quasi-static strain rates, as opposed to many crossing shear bands that were observed at dynamic strain rates (their tensile results are included in Fig. 5 as the points marked with the symbol "a"). We speculate that when very high deformation rates are applied to a BMG, a single shear band cannot accommodate the imposed deformation quickly enough, as described below.

As deformation is initiated in a BMG, the response is initially elastic, until at some point the yield criterion is satisfied; this criterion has been developed for indentation loading of a Mohr-Coulomb solid by Wright et al. [1]. At the critical stress level, a first shear band is initiated, and, if the applied strain rate is slow, this single shear band can rapidly accommodate the applied strain, leading to a strain burst. In contrast, if the applied strain rate exceeds the rate of relaxation by a single shear band, then the first band will still be operating as the stress level exceeds the yield criterion again, and a second shear band is initiated. At very rapid rates of loading, we imagine that many shear bands would be required at every instant in order to accommodate the applied strain; instead of observing single shear band activity, a virtual "field" of shear bands would continuously accommodate the imposed deformation.

The above explanation is consistent with all of the observations of the present work, as well as the assembled literature data presented in Fig. 5. It can also explain why prior investigators using Zr-based BMGs (e.g., Refs. [1,18]), did not observe significant serrations in their *P-h* curves, but did observe shear bands on the surface of the specimens after indentation. Since serrated flow is only pronounced in the Zr-BMG alloys at the lowest indentation strain rates (Figs. 1 and 4), typical indentation rates may well fall in the high-rate regime of continuous yielding carried by multiple shear bands simultaneously. Furthermore, we also note that the "natural" shear rate of shear bands is not expected to be a single value, but one determined somewhat stochastically by local arrangements of atoms. The shear rate during each serration would be affected by the local free volume, as well as short- or medium-range ordering (either geometric or chemical) of the local constituents. Since shear bands may also produce ordering or even crystallization in BMGs [24], shear band formation may also depend on the local deformation history. These stochastic qualities can explain the data in Fig. 4, where the upper bound (given by the dashed lines) may represent an intrinsic limit to the speed of shear band formation, but where the considerable scatter below that limit is due to the random nature of the glassy atomic structure. Changes in local structure may also give rise to strong dependencies on cooling rate during casting, as well as to compositional details; serrated flow may be significantly different for various batches of the same alloy.

Finally, we note that our results may also have implications for deformation modeling of BMGs

and nanocrystalline metals. For example, molecular dynamics (MD) simulation commonly employs strain rates near 10^8–10^9 s^{-1} [54], well above the transition we have observed from discrete to continuous plasticity in BMGs (near 10^{-1} to 10 s^{-1}). MD should therefore only be able to access plasticity events involving multiple simultaneous shear bands, and may not be suitable for the study of serrated flow in BMGs. A similar argument may also apply to nanocrystalline metals, which contain a high volume fraction of disordered grain boundary phase that is commonly viewed as amorphous. As the grain size of these materials is reduced below ~10 nm, they undergo a transition to a largely amorphous structure, whose mechanical properties and deformation mechanisms should approach those of an amorphous metal [55,56]. Thus, one may expect that shear banding will occur in nanocrystalline metals, and the rate dependencies discussed in this work are expected to apply to those materials as well.

5. Summary and conclusions

Four bulk metallic glasses (BMGs) have been subjected to instrumented nanoindentation loading, including Pd-40Ni-20P, Pd-30Cu-10Ni-20P, Zr-10Al-10Ni-15Cu, and Zr-10Al-14.6Ni-17.9Cu-5Ti. The salient results of this work are listed below:

- All four of these BMGs exhibit similarities in their load-displacement (*P-h*) curves, specifically in regard to the phenomenon of serrated flow. During nanoindentation, serrated flow is manifested as a series of discrete strain bursts, referred to as the "pop-in" phenomenon. Previous studies have correlated these discontinuities in the *P-h* curve with the operation of individual shear bands; here we demonstrate the generality of serrated *P-h* curves for four different BMG alloys.
- Serrated flow is found to be a strong function of the rate of deformation, with more rapid indentations suppressing—and slower indentations promoting—prominent serrations. For each alloy, a critical indentation strain rate was identified, above which load serrations apparently do not occur. This threshold strain rate was somewhat different for each alloy, suggesting the importance of local atomic arrangements and composition on shear banding. The present results span about five orders of magnitude in strain rate, and shed light upon the trends observed in prior studies of BMGs under various modes of loading.
- The transition from serrated to non-serrated flow is shown to involve a change in the character of plasticity for BMGs. Specifically, for slow indentation of the Pd-30Cu-10Ni-20P alloy, we demonstrate that all of the plastic deformation occurs solely through individual load serrations; all of the plasticity arises from the discrete operation of individual shear bands. Conversely, at high indentation rates, none of the measured plastic strain can be attributed to load serrations. The transition between the discrete and continuous extremes occurs over four decades of strain rate in Pd-30Cu-10Ni-20P, and similar trends are observed for the other BMGs. However, for these alloys much slower deformation rates will be required to effect a transition to fully discrete serrated plastic flow.

Acknowledgements

This work was performed under the auspices of the U.S. Department of Energy under contract W-7405-Eng-48 with the University of California, Lawrence Livermore National Laboratory. Experimental materials were generously supplied by Dr. C. T. Liu (Oak Ridge National Laboratory) and Dr. Y. Kawamura (Kumamoto University, Japan).

References

[1] Wright WJ, Saha R, Nix WD. Mater Trans JIM 2001;42:642.
[2] Pampillo CA. J Mater Sci 1975;10:1194.
[3] Pampillo CA, Chen HS. Mater Sci Eng 1974;13:181.
[4] Donovan PE. Acta Mater 1989;37:445.
[5] Kimura H, Masumoto T. Phil Mag 1981;A44:1005.
[6] Kimura H, Masumoto T. Phil Mag 1981;A44:1021.
[7] Kimura H, Masumoto T. Acta Metall 1980;28:1663.

[8] Kimura H, Masumoto T. Acta Metall 1980;28:1677.
[9] Wright WJ, Schwarz RB, Nix WD. Mater Sci Eng 2001;A319-321:229.
[10] Kimura H, Masumoto T. Acta Metall 1983;31:231.
[11] Bruck HA, Christman T, Rosakis AJ, Johnson WL. Scripta Metall Mater 1994;30:429.
[12] Pekarskaya E, Kim CP, Johnson WL. J Mater Res 2001;16:2513.
[13] Donovan PE. Mater Sci Eng 1988;98:487.
[14] Lowhaphandu P, Montgomery SL, Lewandowski JJ. Scripta Mater 1999;41:19.
[15] Flores KM, Dauskardt RH. Mater Sci Eng 2001;A319-321:511.
[16] Flores KM, Dauskardt RH. Acta Mater 2001;49:2527.
[17] Liu CT, Heatherly L, Easton DS, Carmichael CA, Schneibel JH, Chen CH et al. Metall Mater Trans 1998;29:1811.
[18] Vaidyanathan R, Dao M, Ravichandran G, Suresh S. Acta Mater 2001;49:3781.
[19] Inoue A, Zhang W, Zhang T, Kurosaka K. J Mater Res 2001;16:2836.
[20] Mukai T, Nieh TG, Kawamura Y, Inoue A, Higashi K. Scripta Mater 2002;46:43.
[21] Chen HS. Scripta Metall 1973;7:931.
[22] Neuhauser H. Scripta Metall 1978;12:471.
[23] Flores KM, Dauskardt RH. J Mater Res 1999;14:638.
[24] Kim JJ, Choi Y, Suresh S, Argon AS. Science 2002;295:654.
[25] Golovin YI, Ivolgin VI, Khonik VA, Kitagawa K, Tyurin AI. Scripta Mater 2001;45:947.
[26] Corcoran SG, Colton RJ, Lilleodden ET, Gerberich WW. Phys Rev 1997;B55:R16057.
[27] Bahr DF, Kramer DE, Gerberich WW. Acta Mater 1998;46:3605.
[28] Suresh S, Nieh TG, Choi BW. Scripta Mater 1999;41:951.
[29] Gouldstone A, Koh H-J, Zeng K-Y, Giannakopoulos AE, Suresh S. Acta Mater 2000;48:2277.
[30] Gouldstone A, VanVliet KJ, Suresh S. Nature 2001;411:656.
[31] Schuh CA, Nieh TG, Kawamura Y. J Mater Res 2002;17:1651.
[32] Kato H, Kawamura Y, Inoue A, Chen H-S. Mater Sci Eng 2001;A304-A306:758.
[33] Nieh TG, Wadsworth J, Liu CT, Ohkubo T, Hirotsu Y. Acta Mater 2001;49:2887.
[34] Wang JG, Choi BW, Nieh TG, Liu CT. J Mater Res 2000;15:913.
[35] Wang JG, Choi BW, Nieh TG, Liu CT. J Mater Res 2000;15:798.
[36] Kawamura Y, Kato H, Inoue A, Masumoto T. Mater Sci Eng 1996;A219:39.
[37] Bérces G, Chinh NQ, Juhász A, Lendvai J. J Mater Res 1998;13:1411.
[38] Chinh NQ, Horváth G, Kovács Z, Lendvai J. J Mater Sci Eng 2002;A324:219.
[39] Bérces G, Chinh NQ, Juhász A, Lendvai J. J. Acta Mater 1998;46:2029.
[40] Nix WD. private communication 2001.
[41] Lam DCC, Chong ACM. Mater Sci Eng 2001;A318:313.
[42] Sargent PM, Ashby MF. Mat Sci Technol 1992;8:594.
[43] Lucas BN, Oliver WC. Metall Mater Trans 1999;30A:601.
[44] Poisl WH, Oliver WC, Fabes BD. J Mater Res 1995;10:2024.
[45] Mattern N, Kuhn U, Hermann H, Ehrenberg H, Neuefeind J, Eckert J. Acta Mater 2002;50:305.
[46] Nieh TG. unpublished research, Lawrence Livermore National Laboratory, 2002.
[47] Storakers B, Larsson P-L. J Mech Phys Solids 1994;42:307.
[48] Mayo MJ, Nix WD. Acta Metall 1988;36:2183.
[49] Li JCM. Mater Sci Eng 2002;A322:23.
[50] Mukai T, Nieh TG. unpublished research, Lawrence Livermore National Laboratory 2002.
[51] Oliver WC, Pharr GM. J Mater Res 1992;7:1564.
[52] Johnson KL. Contact Mechanics. Cambridge, UK: Cambridge University Press, 1985.
[53] Wang LM, Sun LL, Wang WH, Wang RJ, Zhan ZJ, Dai DY, Wang WK. Appl Phys Lett 2000;77:3734.
[54] Raabe D. Computational Materials Science. Weinheim: Wiley-VCH, 1998.
[55] Nieh TG, Wadsworth J. J. Scripta Metall Mater 1991;25:955.
[56] Wang N, Palumbo G, Wang Z, Erb U, Aust KT. Scripta Metall Mater 1993;28:253.